THE AMERICAN SOCIETY OF MECHANICAL ENGINEERS
Three Park Avenue, New York, N.Y. 10016-5990

99-GT-418

FLOW FIELD MEASUREMENTS IN AN ANNULAR GAS TURBINE EXHAUST DIFFUSER WITH STRUTS

Umberto Desideri and Stefano Ubertini
Dipartimento di Ingegneria Industriale, Università di Perugia
Via G. Duranti 1A/4 – 06125 Perugia, Italy
Phone+Fax +39 0755852736
e-mail: desideriu@asme.org

ABSTRACT

This paper presents the velocity and turbulence characteristics of the flow in an annular diffuser, which is a model of a gas turbine exhaust diffuser with six struts. The diffuser where the measurements were made is a scaled down model of a 10 MW gas turbine, built by GE/Nuovo Pignone.

In a previous paper (Desideri and Manfrida, 1995) 2-D turbulence and velocity measurements were presented with axial inlet velocity conditions.

In this paper a more detailed 3-D analysis of the design and off design behavior of the diffuser is presented. Turbulence characteristics were determined by means of two hot split-film probes, which allowed measuring axial, radial and tangential components of the mean velocity and their fluctuating components. The measuring point is moved inside the diffuser by means of two step-motors, which allow the rotation of the hub and the radial displacement of the probe.

Off-design behavior of the annular diffuser was determined by changing the inlet velocity angle of 10° from axial direction. The effect of swirl on the performance of the diffuser will be presented.

Turbulence microscales were also calculated in regions of interest inside the diffuser, with particular attention to the strut wake.

NOMENCLATURE

g(r)	lateral correlation coefficient
U	axial velocity component = U_m+u
V	tangential velocity component = V_m+v
W	axial velocity component = W_m+w
α	Temperature coefficient
ε	Dissipation rate
η	Kolmogorov length scale
λ	Taylor's microscale
ν	Cinematic viscosity

INTRODUCTION

Global parameters and equations, which correlate static and total pressure at inlet and outlet, are generally used to determine diffusers' performance. The design of diffusers is based on performance maps, such as pressure recovery and pressure loss maps (Japikse, 1986). In the cases, where the length of the diffuser is not a primary constraint, diffuser angles are determined from performance maps with ample margins to avoid separation phenomena. Design based on performance maps is easy, but maps do not consider the presence of obstacles inside the diffusers and the distortion of the flow at inlet.

The performance of diffusers located after a turbomachine (axial compressors and turbines) is influenced by the highly turbulent flow at inlet. Therefore the knowledge on the inner flow behavior is required, in order to predict the flow field of the diffuser (Pfeil and Going, 1987). It is no longer appropriate to treat the diffuser, as an isolated component in the design process, but the whole diffusing system including the turbomachine has to be taken in account (Raab, et al., 1996). In fact, the increased level of turbulence, caused by the blades of the turbine upstream of an exhaust diffuser, can sometimes improve the pressure recovery (Zierer, 1995). All the above reasons push towards a more detailed analysis of diffusers and mainly of their interaction with the flow coming from the turbine or the compressor.

The exhaust diffuser of a gas turbine often features structural elements (struts), which are necessary to support the shaft. The presence of these objects influences the flow field and increases pressure losses, even though they are generally designed using aerodynamic profiles. Putting some attention to the design of the struts can effectively modify the structure of the vortexes shedding from the strut, and improve diffuser perfromance (Fric, et al., 1996).

Experimental investigations made by Norris, et al., (1998) within a diffusing S-shaped duct show that the presence of a row of struts has two detrimental effects:

Presented at the International Gas Turbine & Aeroengine Congress & Exhibition
Indianapolis, Indiana — June 7–June 10, 1999

- They cause a blockage and consequently the flow accelerates, reducing the diffusion;
- They increase the size of the separation bubble.

This paper presents the 3D description of the flow field of a model of an exhaust diffuser for gas turbines, including 24 blades at inlet that simulate the effect of the turbulence induced by the last stage of the upstream turbine.

DIFFUSER MODEL

The aim of this paper is the characterization of the flow in a diffuser model built by Nuovo Pignone S.p.A. reducing in 0.35:1 scale the exhaust diffuser of a PGT10 gas turbine.

The inlet of the model has been shaped in order to prevent flow separation in the first part of the diffuser. The shell is made up of transparent Plexiglas to check the position and the movements of the probes. At the inlet section there are 24 guide vanes which generate a wake similar to that produced by the blades of the last turbine rotor. The guide vanes can be rotated about their axis to simulate non-axial off-design flow at turbine outlet.

The interesting part in the characterization of the diffuser is the distortion of the flow produced by the presence of six high-solidity struts, which support one of the shaft bearings and have piping oil supply inside for bearings lubrication of the gas turbine.

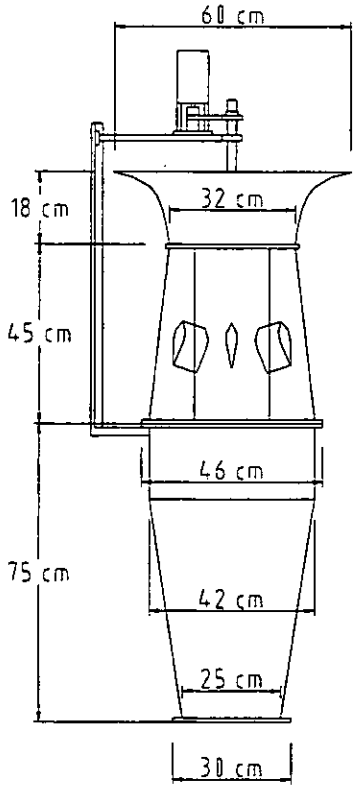

Figure 1: Model of gas turbine exhaust diffuser.

The inner and outer diameters of the inlet section are 190 mm and 320 mm. Axial length of the diffuser is 340 mm with an outer diameter at outlet of 420 mm. The resulting conicity of the shell is 1: 0.28. The area ratio of the diffuser is 1.53 and the length/wide ratio is 2.01 (Fig. 1). To keep geometric similarity of the model with the GT diffuser, the area ratio is maintained the same along the axis in both the model and the GT diffuser.

The model was designed to operate in geometric and Reynolds number similarity with the GT diffuser. The GT diffuser operates with 41.3 kg/s at 462 °C and has a Reynolds number higher than 10^6. The Reynolds number in the model is high enough ($Re > 6\times10^5$) to assume similar flow conditions in the GT diffuser and in the 35% scale model.

The inner hub is a stainless steel cylinder rotatable over 360°. Four automated carriages for probe radial movements are mounted inside the inner hub, which has four holes to position the probes into the flow field. The carriages motion is automated by small geared stepping motors (Fig. 2). Another stepping motor has the function of rotating the hub in order to realize the circumferential movement of the probes. A 2-channels MSTEP-5 motor management board permits the control of the stepping motors by personal computer

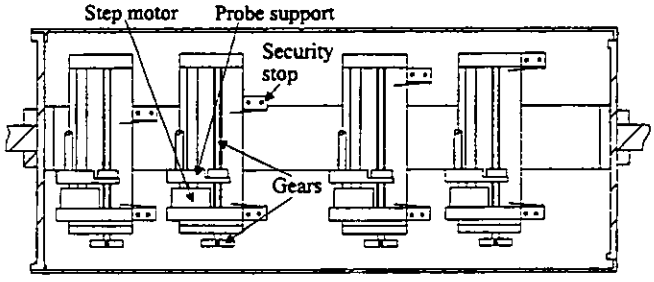

Figure 2: Carriages for the movement of test probes inside the inner hub.

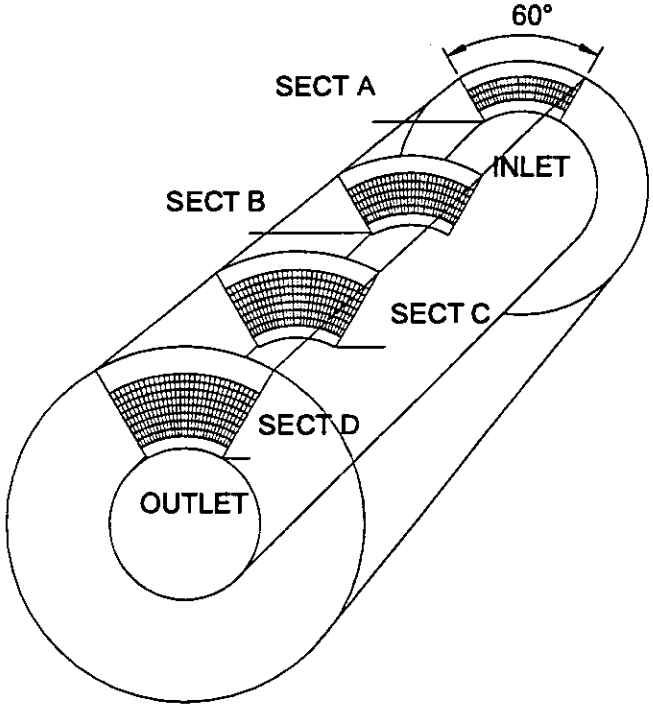

Figure 3: Measurement sections arrangement.

MEASUREMENT SECTIONS

The measurement sections, shown in Fig. 3, are named as section A, B, C and D. Section A is just behind the guide vanes; sections B and C allows the characterization of the flow in front and behind the strut. Section D is the section at outlet.

Since the inner hub diameter is constant over the entire length, it is also possible to move the measurement sections in the axial direction. Figure 3 also shows the position of the measuremeni points in each section. The first radial point of acquisition is 15 mm far from the inner hub and it corresponds to 0 mm radial position in all the plotted graphs.

The radial movement of the probe is made up of 10 mm steps, to a safety distance from the shell. 31 angular positions correspond to every radial one, covering a sector of 60° containing one strut in the middle. Results have been produced for a 60°sector because the flow field repeats itself every 60°. The 60° sector was chosen in the upper part to avoid any interaction with the step-motor and its support, which disturb the flow behind in the lower part of the model.

The model is connected to a wind tunnel with a 22 kW centrifugal-flow industrial fan. The flow rate is controlled by a sluice gate, positioned 3.40 m before the exhaust.

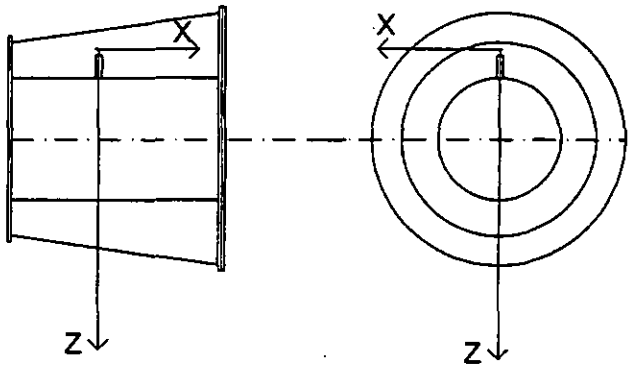

Figure 4: Reference measurement system.

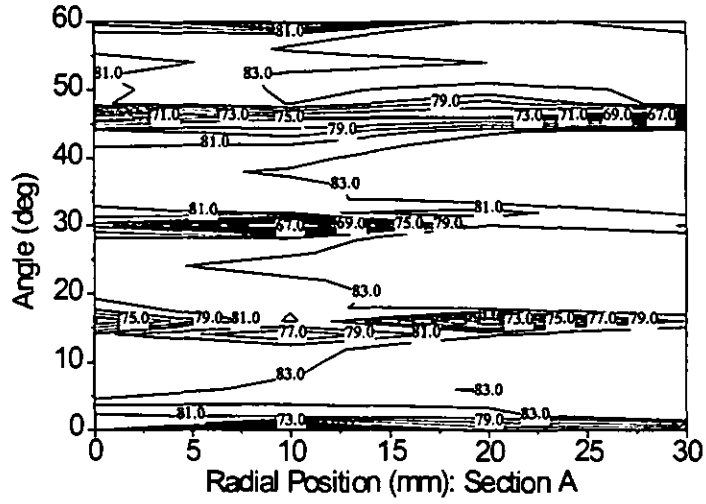

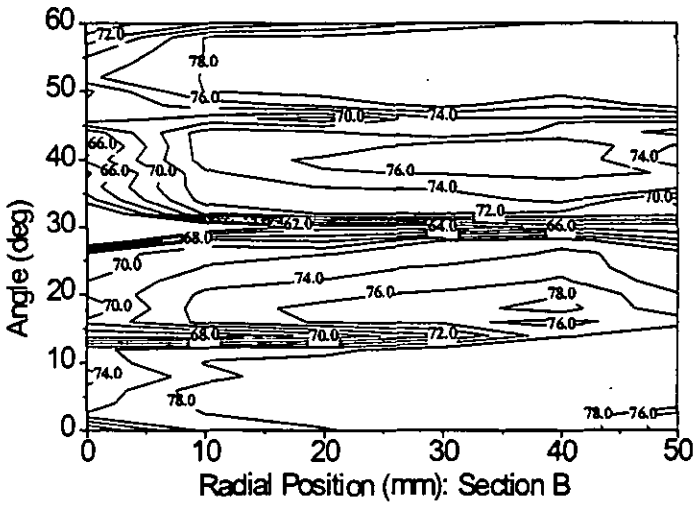

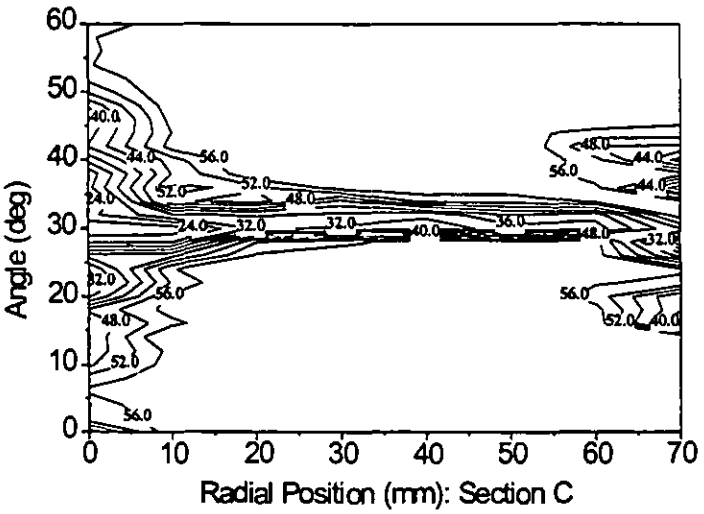

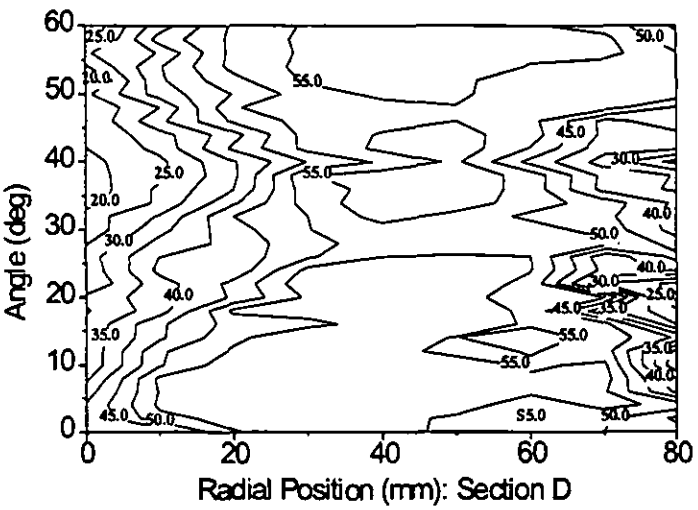

Figure 5: Contour plots of axial velocity U_m (m/s) with straight guide vanes.

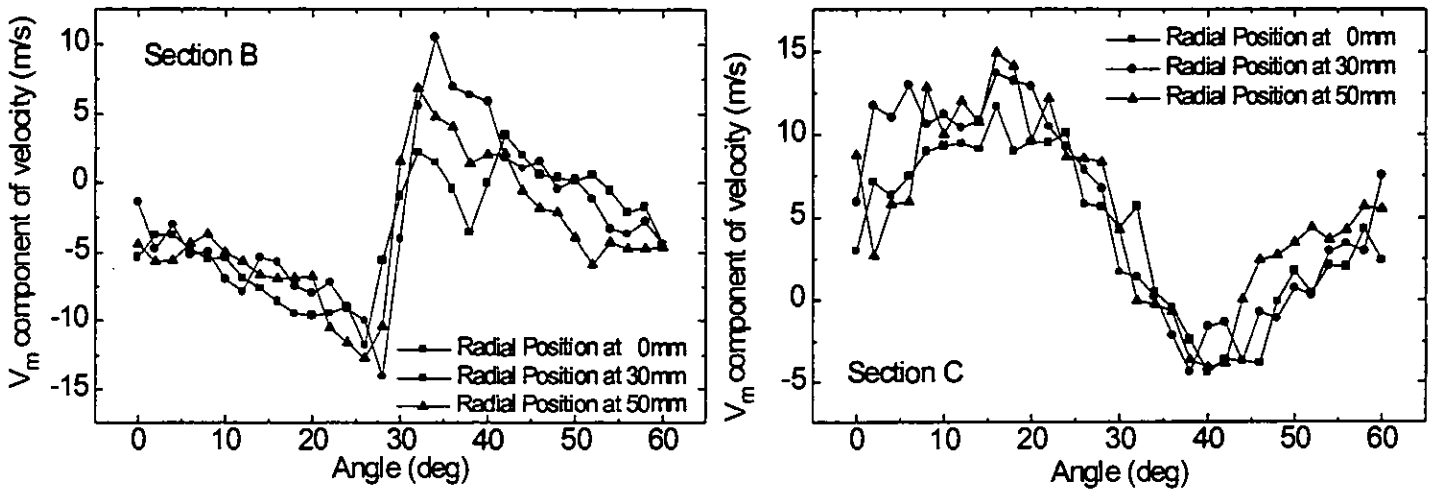

Figure 6: V_m velocity component vs. angular position at sections B and C.

MEASUREMENT TECHNIQUES

The 3D characterization of the diffuser flow was made by using two types of split-film probes:

- DANTEC 55R56 split-film probe with R_{20} = 4.5 Ω for one film and 4.8 Ω for the other and α_{20} = 0.0039 for one film and 0.0041 for the other
- DANTEC 55R57 split film probe with R_{20} = 5.27 Ω and 4.57 Ω, and α_{20} = 0.0042 and 0.0041.

The 55R57 probe allows the measurement of the x and y components of the velocity vector, whereas the 55R56 measures the components on the x-z plane (Fig. 4).

The measurements with the two probes are made with the same flow velocity in the tunnel at two different times, so it is not possible to correlate turbulence quantities obtained on the x-y plane to those on the x-z one.

The probes were connected to a dual-channel anemometric system by A.A. Labsystems, which includes amplification and filtering for each channel. The anemometer output was then transmitted to a sampling board and a PC elaborated the results. The sampling board used is a Metrabyte DAS-1600, which features 16 channel and a 12-digit A/D converter. The maximum acquisition rate is 100 kHz.

The similarity of flow conditions among measurements made at different times is guaranteed by keeping the wind tunnel flow rate constant. This assumption also allows making measurements with only one probe at a time thus avoiding flow interaction between probes simultaneously located in the flow field.

EXPERIMENTAL RESULTS

The flow field of the diffuser model was studied in two different conditions:

- with straight inlet blades;
- with 10° inclined inlet blades.

Figure 5 shows the contour plots of the axial component of velocity at the four sections with straight inlet blades.

The presence of the guide vanes can be easily detected in the plot of section A. A flow deviation and a reduction of the axial velocity, U_m, is evident at 15°, 30° and 45°, which are the angular positions of the guide vanes.

In section B the downstream strut at 30° causes a strong deviation of the fluid with a significant reduction of the axial velocity. The presence of the guide vanes at 15° and 45° is still traceable. The y-component velocity graph, shown in Fig. 6, confirms the deviation caused by the presence of the strut.

The plot of section C shows a wide area of low axial velocity, caused by the wake of the strut. Approaching the inner hub, axial velocity slows down and this can be mainly attributed to the growth of the boundary layer. The presence of the guide vanes is still detectable. It seems that the interaction between the guide vanes and the strut wakes causes the onset of the flow separation at the shroud. The Y-component of velocity graph (Fig. 6), shows how the flow reattaches behind the strut.

In section D, the growth of the boundary layer is more evident, since the axial velocity decreases from 55 m/s, at mid-span, to 20 m/s near the hub. A clear zone of separation can be observed between the strut and the guide vanes close to the shroud.

The V_m and W_m components of the velocity vector are shown in Figs. 7 to 10. V_m and W_m components are very small in Section A (Fig. 7). Span-wise deviations from the axial velocity are due to the presence of guide vanes. Since the thickness of the guide vanes is 5 mm and they present a rounded trailing edge, the V_m component is always in the interval ±4 m/s. The W_m component is generally zero, except along the guide vanes, where a slight upward direction from the hub to the shroud can be observed.

Before the strut there is a significant deviation in the V_m direction, with a left-wise direction on the left of the strut and a right-wise direction on the other side (Fig. 8). Near the hub the W_m component is negative (upward to the center of the section), whereas near the shroud it is positive, i.e. directed downward. This characteristics is the same along all the hub and the shroud, but the highest W_m component can be found along the sides of the strut (at 30°) and along the wakes generated by the guide vanes at 15° and 45°.

In section C a secondary flow is quite evident on the sides of the main wake generated by the strut. The V_m component is positive on both sides of the strut in the region near the hub from 0 to 35 mm, and negative near the shroud (Fig. 9). If we combine this component with the W, two vortexes with counterclockwise direction can be observed.

In section D (Fig. 10), the flow is mainly redirected along the axis and V_m and W_m components have almost disappeared. There still remains a slight V_m component due to the reattachment of the flow behind the strut and the W_m component due to the development of the boundary layer.

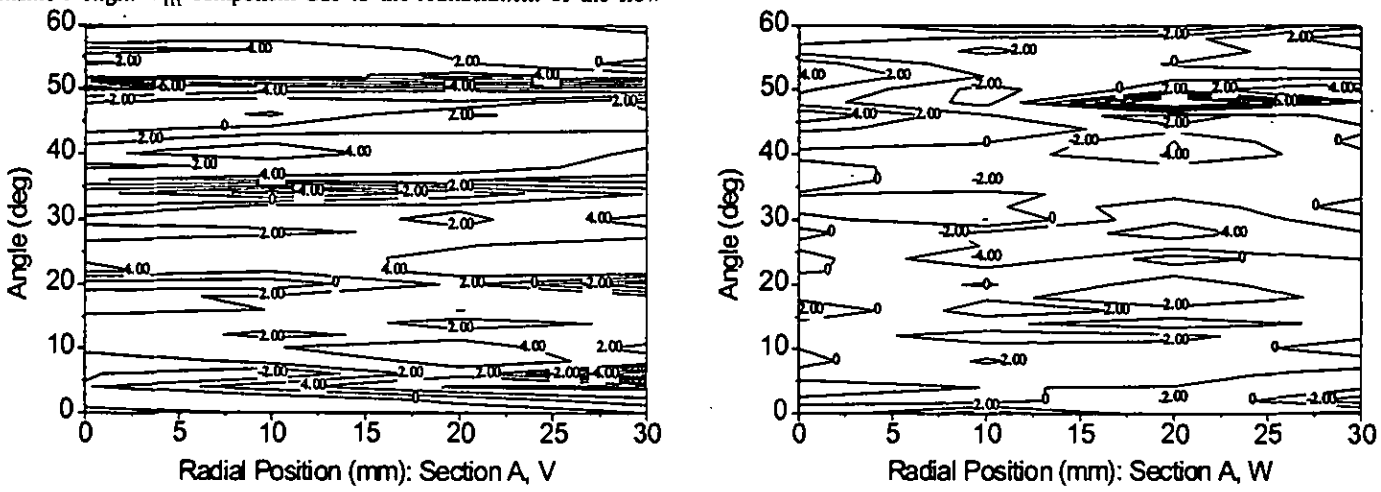

Figure 7: Contour plots of the V_m and W_m velocity components (m/s) with straight guide vanes in section A.

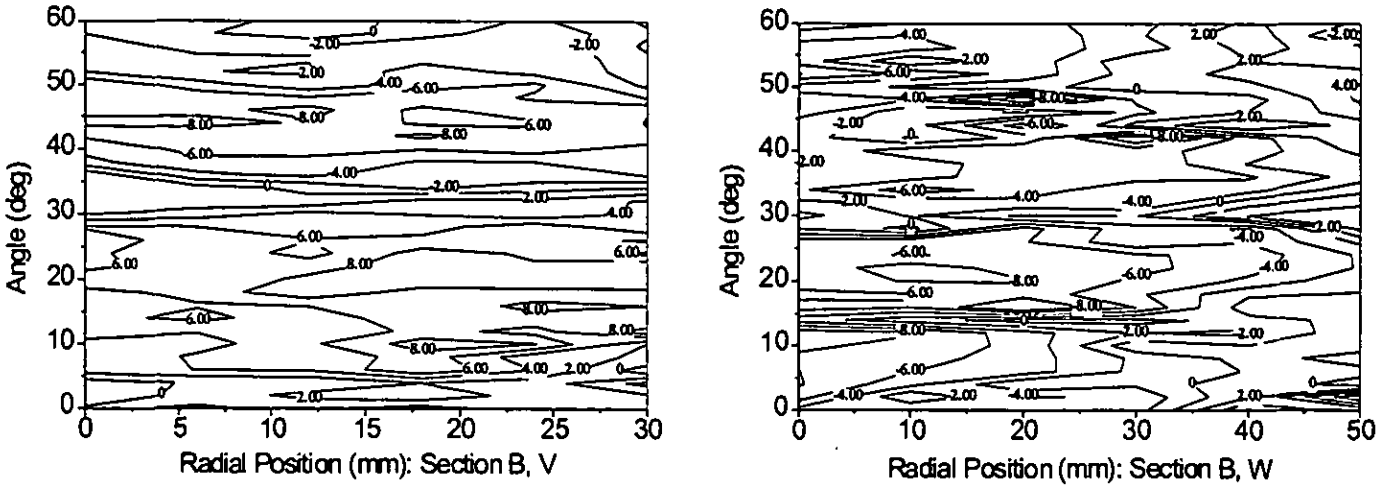

Figure 8: Contour plots of the V_m and W_m velocity components (m/s) with straight guide vanes in section B.

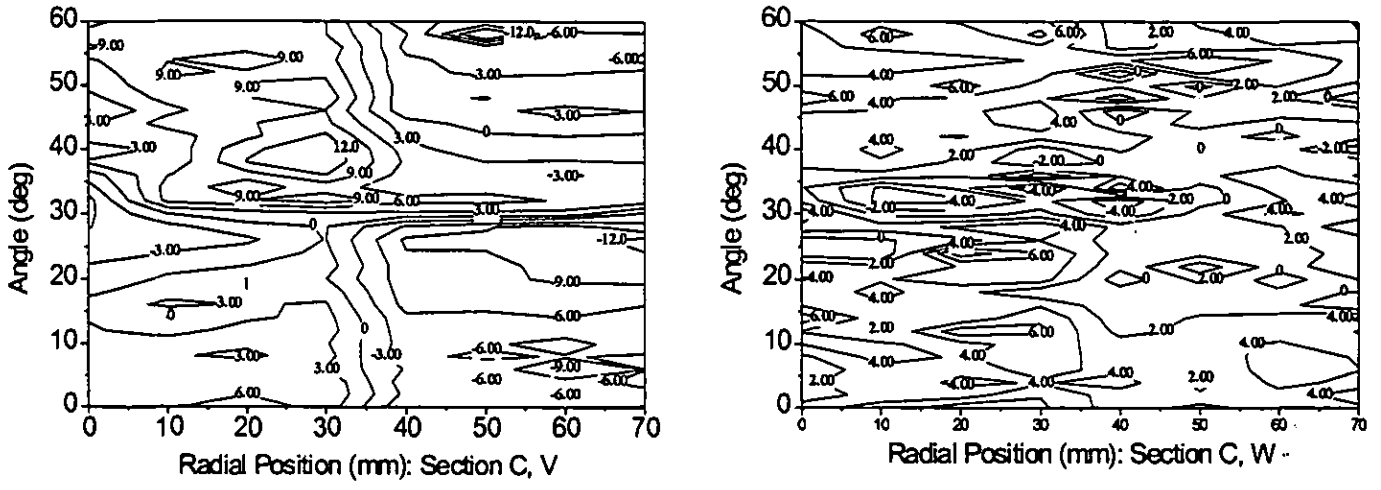

Figure 9: Contour plots of the V_m and W_m velocity components (m/s) with straight guide vanes in section C.

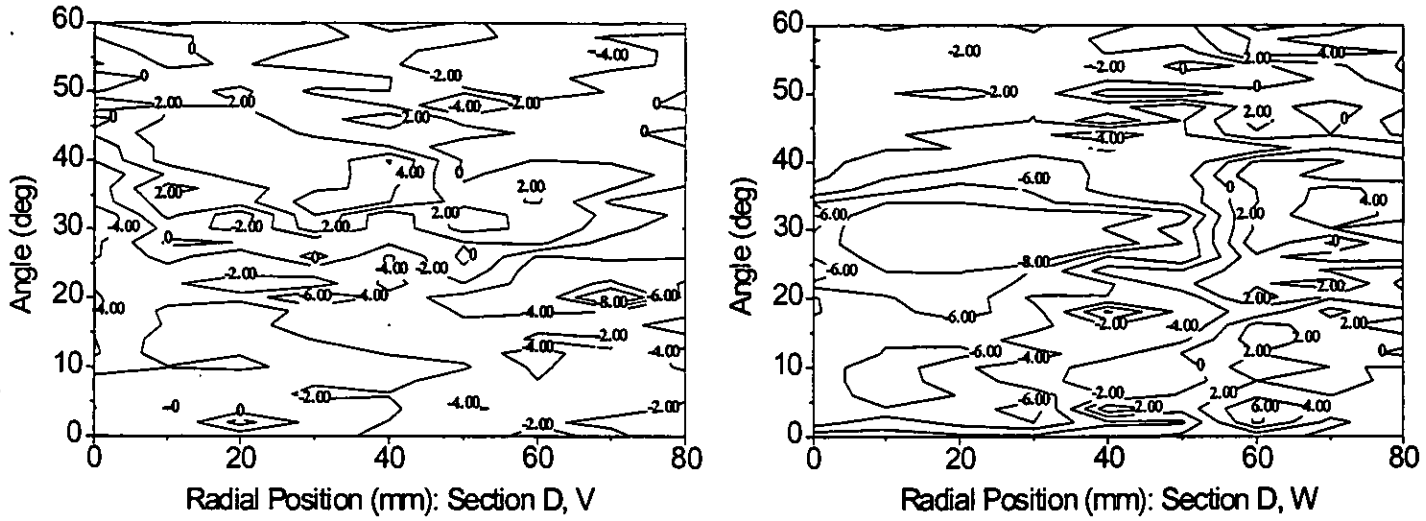

Figure 10: Contour plots of the V_m and W_m velocity components (m/s) with straight guide vanes in section D.

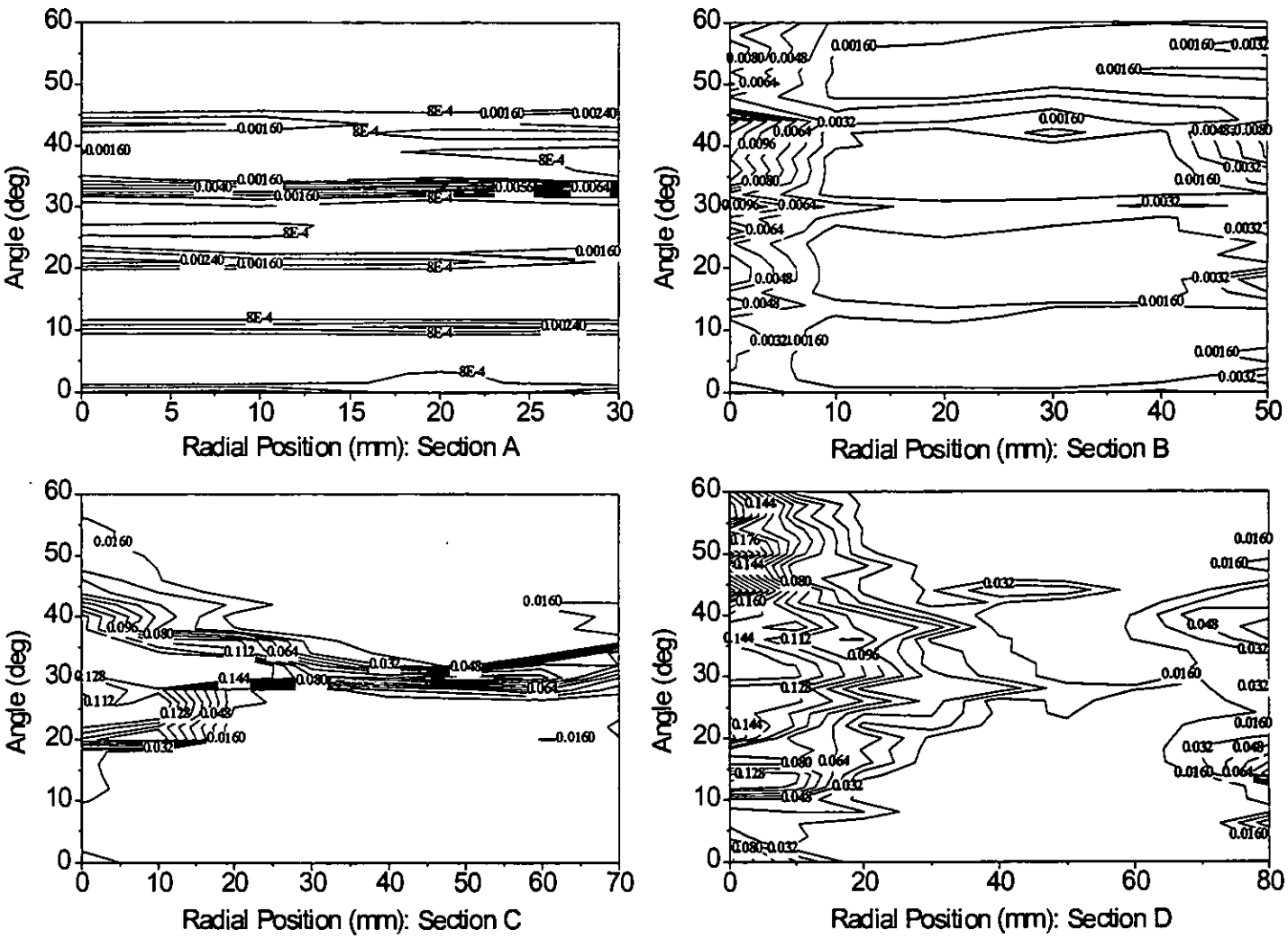

Figure 11: Contour plots of the axial fluctuating velocity component, u, (straight guide vanes).

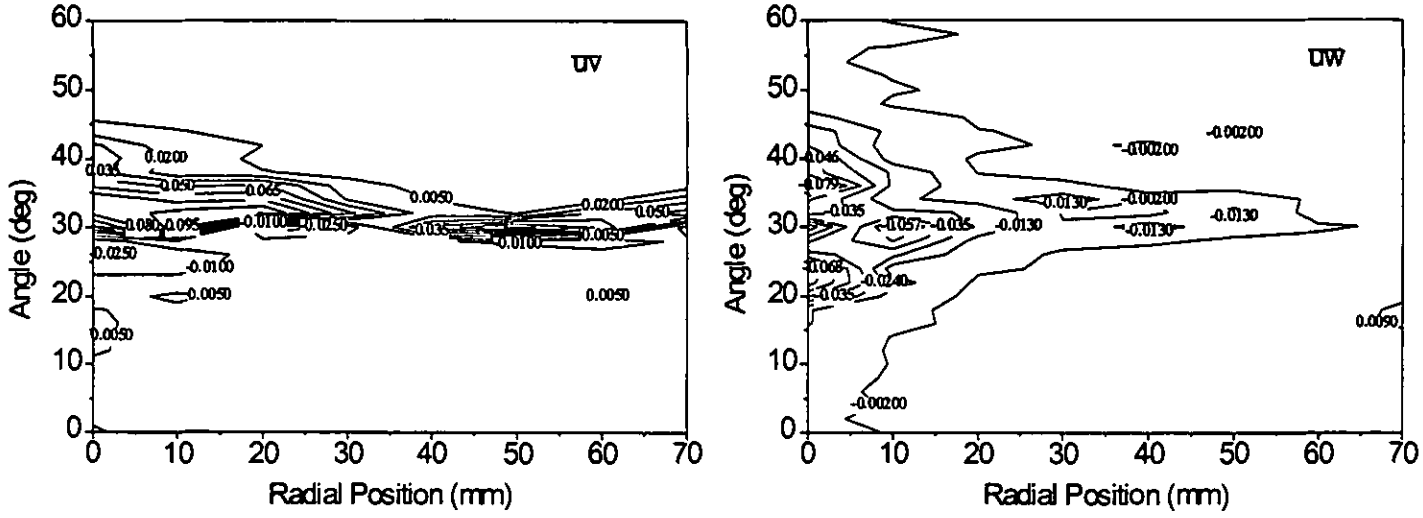

Figure 12: Contour plots of the product of tangential components of velocity fluctuations (straight guide vanes)

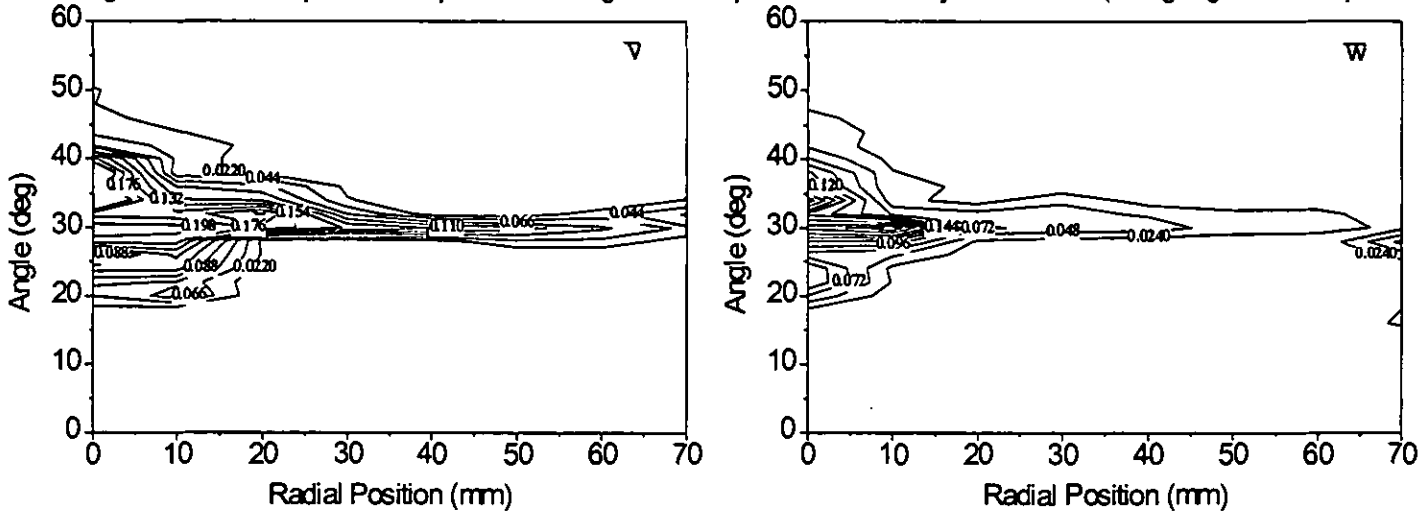

Figure 13: Contour plots of the v and w components of velocity fluctuations (straight guide vanes)

Figure 11 shows the contour plot of the axial component of velocity fluctuations. Measured turbulence quantities are the axial and tangential components of velocity fluctuations and their product in both the xy and the xz-planes. The rms of turbulent components (proportional to Reynolds stresses) is normalized by mean velocity.

Turbulence at inlet increases behind the vanes but it is lower than 1% of average velocity over the largest part of section A. In section B axial velocity fluctuations reach values close to 2-3% only near the inner hub. The tangential components in section A and B are also lower than 2%; this means that turbulence is quite isotropic. The region interested by turbulence higher than 1% is quite narrow behind the guide vanes and the shape of the wakes can be easily traced.

The axial fluctuations are considerably increased in section C, where it reaches 20% behind the strut. From section B to the outlet, it is also evident the growth of the boundary layer, which is more remarkable near the hub, where the width of the passage is smaller. The tangential components of the Reynolds stresses at section C are shown in Fig. 12. Behind the strut, tangential fluctuating components reach 10% . Fluctuating components along y and z, shown in Fig. 13, confirm the high level of turbulence produced by the wake of the strut.

In section D the axial velocity fluctuations are remarkable only near the hub, where they exceed 20%. Instead, the turbulent fluctuations generated by the strut are considerably damped. However, the interaction of the wakes of the strut and the guide vanes near the shroud seems to be the main reason for the development of the boundary layer near the shroud. In the region between the guide vanes, for angles between 0° and 15 and between 45° and 60°, the turbulence is much lower and the boundary layer is not developed as in the region between 15° and 45°.

A second set of measurements was made with the guide vanes rotated of 10°. The differences between this case and the case with straight guide vanes are clear from Fig. 14, where axial velocity contour plots are shown.

In section A, the size of the wakes of the blades at 15°, 30° and 45° are almost double, as each one covers a sector of about 8°. The flow field at section B is characterized by larger slowdown zone, since the axial velocity reaches 70 m/s only in the first and in the last 15° sectors. There is no distinction between the wakes of the guide vanes at 15° and 45° and the stagnation zone produced by the strut.

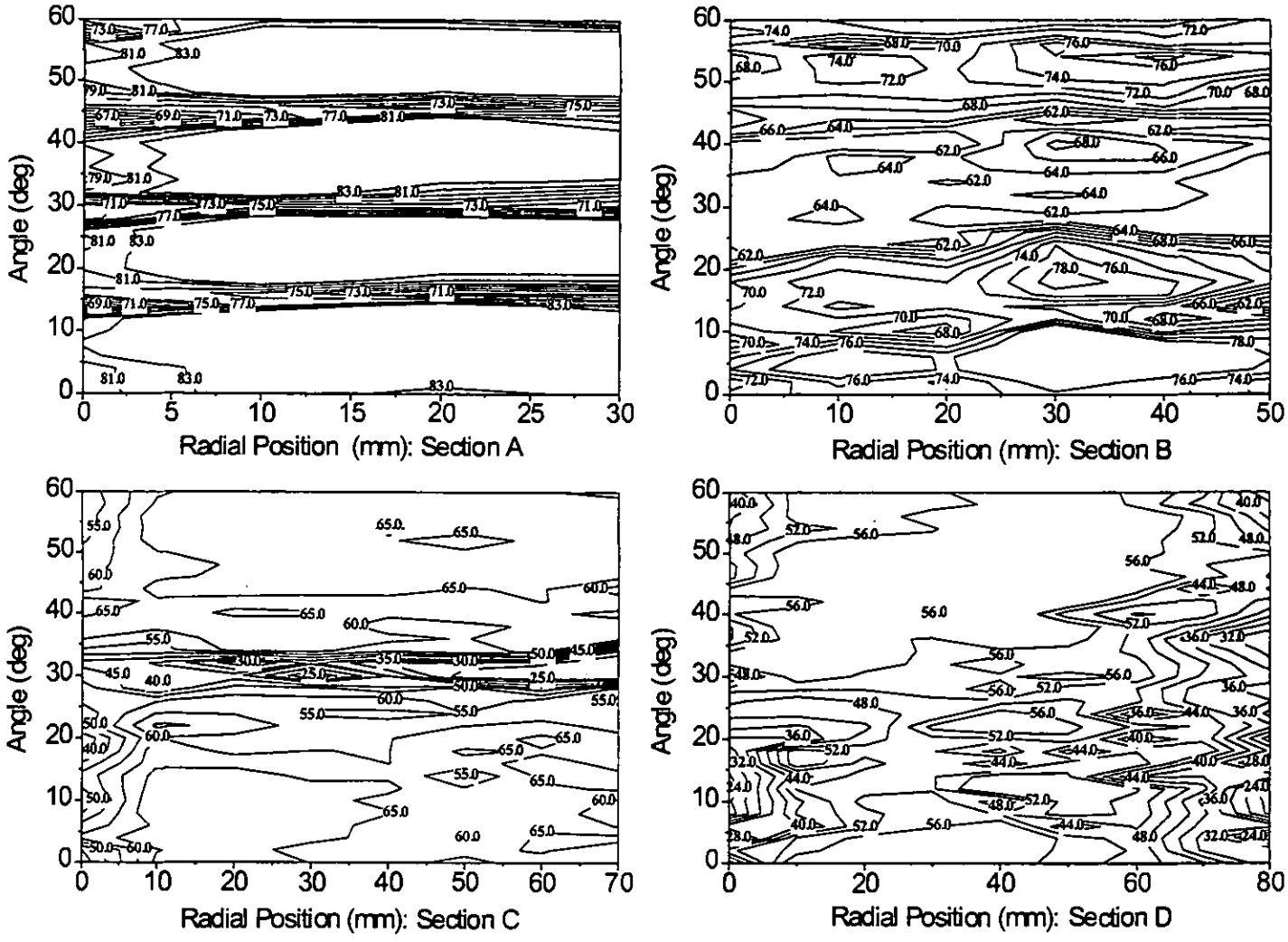

Figure 14: Contour plots of the axial velocity, U_m, (m/s) with inclined guide vanes

In section C the wake of the strut is more evident. The influence of the guide vanes has disappeared and this confirms the strong directional power of the strut.

Moreover, no separation is detected before section D, where a large zone close to the upper hub is characterized by a very low and irregular axial velocity.

The distribution of the axial fluctuating component, shown in Fig. 15, confirms a low level of turbulence in section A and B. In section C the axial Reynolds stress increases behind the strut. The y and z-components of velocity fluctuations follow the case with straight inlet vanes, since they increase behind the strut (8÷15 %).

The tangential components of velocity fluctuation, shown in Fig. 16, point out the anisotropy presence behind the strut, since they reach values close to 10%.

The average level of turbulence is the same of that in the case with straight guide vanes, but the peak values are lower. Moreover, the disappearance of the wakes of the guide vanes damps the separation at the shroud due to the interaction between vanes and struts, especially on the pressure side of the strut.

On the suction side, with the angle ranging from 0° to 15°, a higher turbulence level can be observed near the shroud (Fig. 15, Section D). Therefore, the presence of the strut is not negative for the performance of the strut, when inlet velocity is not axial. The leading edge has such a large curvature and the thickness/chord ratio of the strut is so high that flow with some degrees of incidence is easily straightened.

TURBULENCE MICROSCALE

Turbulence has always all three components of velocity even if the mean flow has only one direction. Therefore, within a turbulent flow, eddies of different sizes govern the energy transfer between the mean flow and the turbulence quantities. The boundary conditions of the flow determine the maximum scale of eddies and vortex stretching causes an energy transfer from large to small eddies. Viscous forces, which dissipate the kinetic energy of the smallest eddies, stop this «cascade» of energy. Therefore, viscous dissipation of turbulent energy determines the scale of the smallest eddies (Bradshaw 1971).

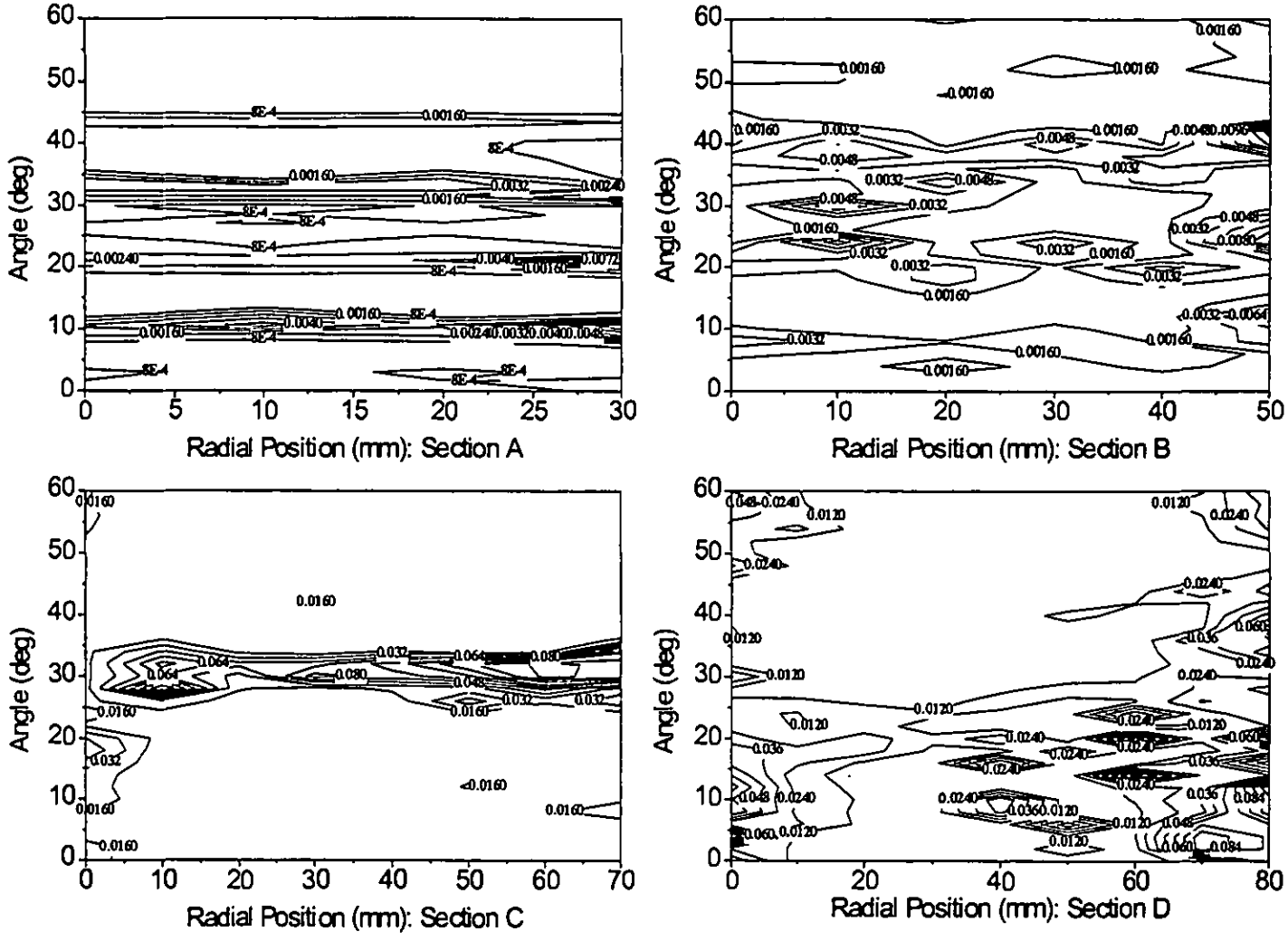

Figure 15: Contour plots of axial fluctuating velocity component (inclined guide vanes)

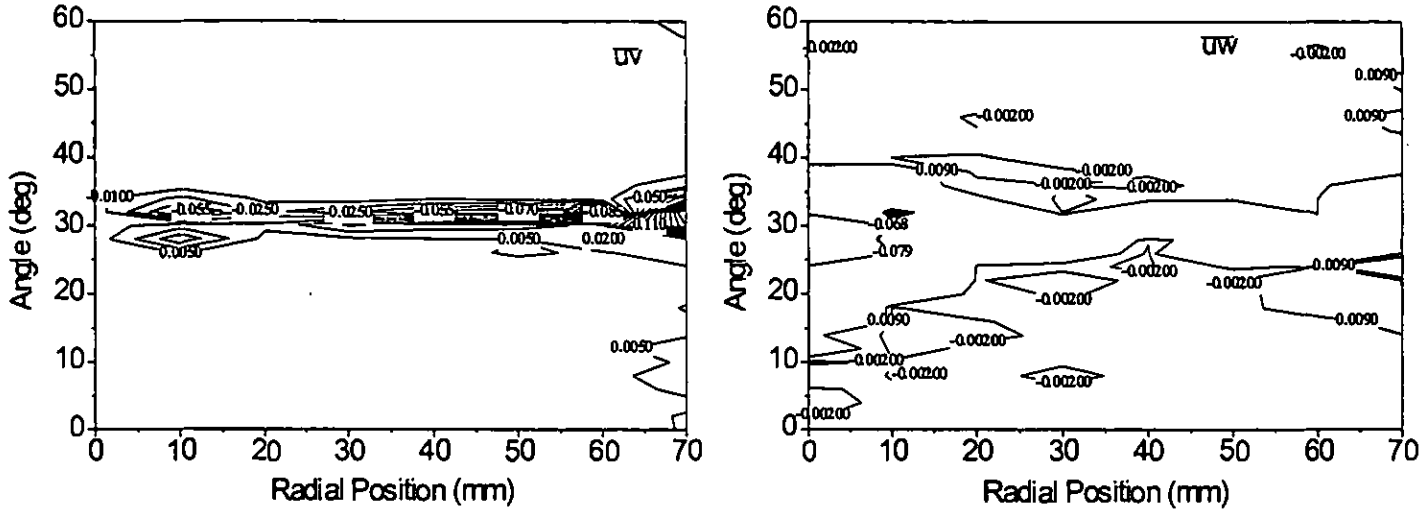

Figure 16: Contour plots of the tangential components of velocity fluctuations (inclined guide vanes).

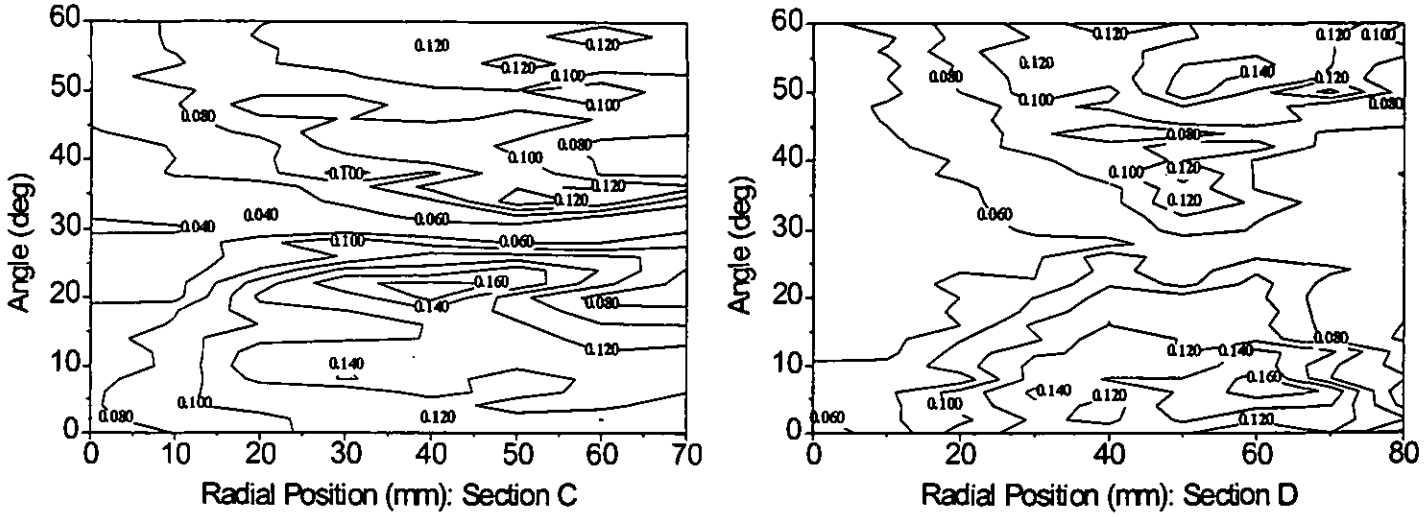

Figure 17: Contour plots of Kolmogorov length scale (mm) with straight guide vanes (finite difference calculation)

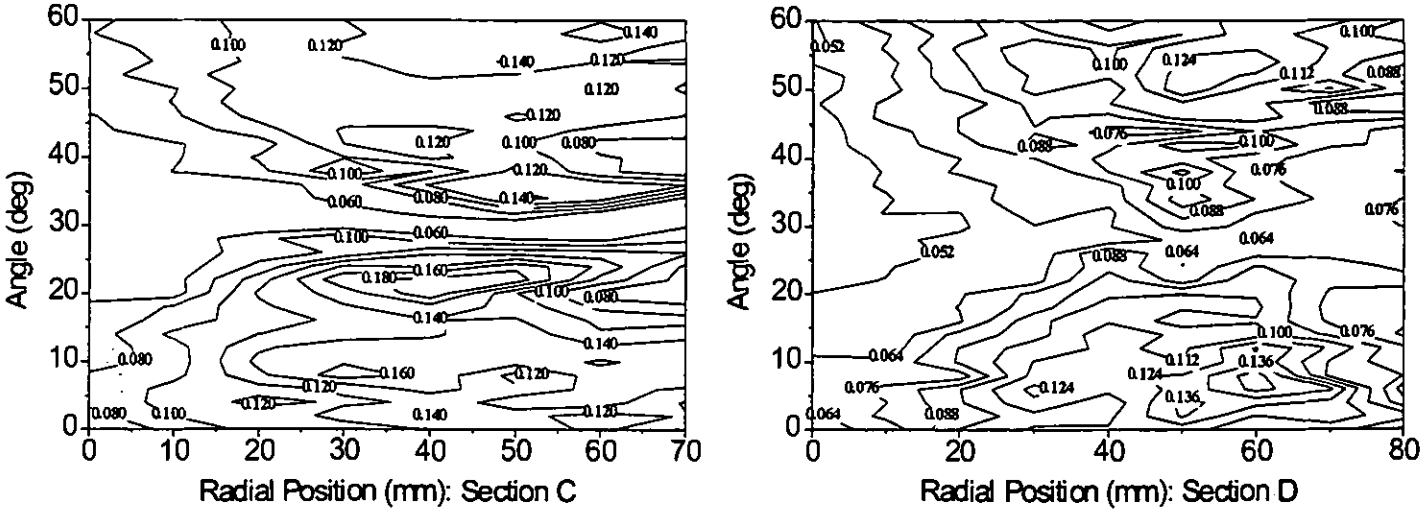

Figure 18: Contour plots of Kolmogorov length scale (mm) with straight guide vanes (by transverse correlation coefficient).

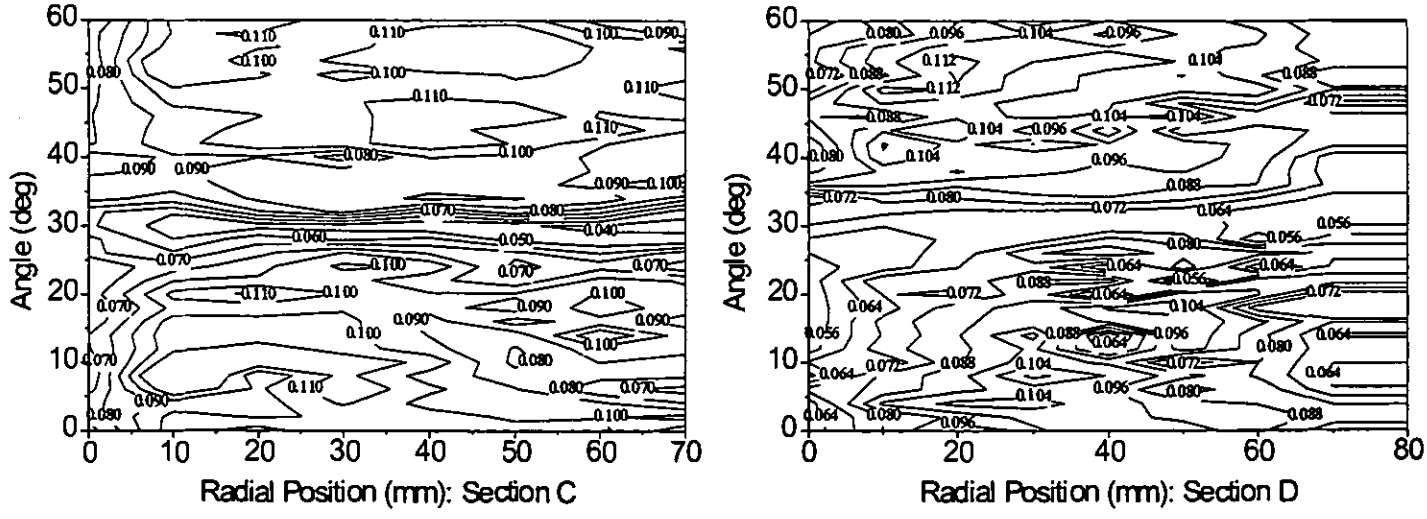

Figure 19: Contour plots of Kolmogorov length scale (mm) with inclined guide vanes.

The Kolmogorov length scale, η, is usually considered as a measure of the "dissipating" eddies:

$$\eta = \left(\frac{\nu^3}{\varepsilon} \right)^{1/4} \tag{1}$$

The Taylor's microscale λ can be used to evaluate η:

$$\lambda = \left[\frac{\overline{u^2}}{\overline{(\partial u/\partial t)^2}} \right] \cdot \overline{U} \tag{2}$$

Taylor's microscale is not a direct measure of either large eddies or of small eddies, but it can be related to both (Bruun 1995).

To determine Kolmogorov length scale, the dissipation rate has to be calculated by using the following expression:

$$\varepsilon = 15\nu \cdot \frac{\overline{u^2}}{\lambda^2} \tag{3}$$

Figures 18 and 19 show the contour plots of η at section C and section D with straight guide vanes. Even if the flow is not isotropic everywhere, they give a good reference of the distribution of the vortex microscale. Taylor's microscale was evaluated in two ways:

- The contour plots of Fig. 17 were determined by a finite difference calculation based on equation (2);
- In the contour plots of Fig. 18, λ was determined by the transverse correlation coefficient as illustrated by Bruun (1995).

The results obtained are practically coincident.

In section C the microscale near the strut tends to reduce, mainly close to the inner hub. As expected where the turbulence is stronger the dissipating eddies are smaller. Close to the shroud there are two areas, characterized by small values of length scale, between the strut and the guide vanes at 15° and 45°. This confirms the hypothesis of separation, due to the interaction of the strut and the guide vanes.

In section D at 30° angular position the microscale is smaller, probably because the wake of the strut is still present even if it is not detectable by measuring the axial velocity only. The separation of the flow at the shroud is pointed out by the small values of eddies dimensions.

Figure 19 shows the Kolmogorov length scale contour plots, with guide vanes rotated of 10°. As seen before, the wake of the strut in section C is narrower. In section D smaller eddies are located close to 30°. The average value of $\eta$is smaller than in section C, probably because the turbulence is spread all over the area.

CONCLUSIONS

A 3D flow field analysis is presented in a model of a gas turbine exhaust diffuser. This has allowed the calculation of the characteristics of the wakes before and after the struts, which support the shaft's bearing in the real gas turbine.

The struts proved to have a strong directional power, even when inlet flow is swirled of 10° from axial direction. However, the struts produce a highly turbulent flow that favors separation between the strut and the vanes and near the hub.

The use of Taylor microscale to detect turbulent flow has produced interesting results, by showing with a good resolution the most important turbulent zones inside the diffuser.

REFERENCES

Bradshaw, P., 1971, "*An Introduction to turbulence and its measurements*", Pergamon Press Ltd., Oxford, UK, pp. 1-17.

Bruun, H.H., 1995, "*Hot Wire Anemometry principles and signal analysis*", Oxford University Press Inc., New York, pp. 62-70.

Desideri, U., Manfrida, G., 1995,"Flow and Turbulence survey for a model of gas turbine exhaust diffuser", *ASME paper 95-GT-139.*

Kline, S.J., Abbott, D.E., Fox, R.W., 1959, "Optimum Design of Straight-Walled Diffusers", *Transactions of the ASME, Journal of Basic Engineering*, pp. 321-330.

Fric, T.F., Villarel, R., Auer, R.O., James, M.L., Ozgur, D., Staley, T.K., 1996, "Vortex shedding from struts in an annular exhaust diffuser", *ASME paper 96-GT-475.*

Norris, G., Dominy, R.G., Smith, A.D., 1998, "Strut influences within a diffusing annular s-shaped duct", *ASME paper 98-GT-425.*

Pfeil, H., Going, M., 1987, "Measurements of the Turbulent Boundary Layer in the Diffuser Behind an Axial Compressor", *Transactions of the ASME, Journal of Turbomachinery*, Vol. 109, pp. 405-412.

Raab, I., Lippert, D., Hennecke, D.K., 1996, "A new concept for the design of turbine diffusers", *ASME paper 96-GT-450.*

Runstadler, P.W. Jr., Dolan, F.X., Dean, R.C. Jr., 1975, "*Diffuser data book*", Creare, TN-186.

Zierer, T., 1995, "Experimental Investigation of the Flow in Diffusers Behind an Axial Flow Compressor", *Transactions of the ASME, Journal of Turbomachinery*, Vol. 117, pp. 231-239.